Armenian e-Science Foundation
&
Yerevan Physics Institute

Marina Grigoryan, Tatevik Poghosyan

Fundamentals of the Strong Interaction Physics

A textbook for undergraduate and graduate studies

Yerevan
2007

CONTENTS

Chapter 1 *Introduction. How the Universe is Organized.*

Over thousand and thousand years of its evolution, *Homo sapiens* was tirelessly aspiring to penetrate into the essence of the surrounding world, to find a proper interpretation of the variety of natural phenomena and to influence on them. Doomed to failure in these endeavors, human being was substituting the knowledge by religion and worshipping to unknown and mysterious. The Gods from the pagan pantheon of ancient Greeks govern the fire, thunders, sea storms, earthquakes…

In the same time, the ancient Greeks have pioneered the abstract studies of the Nature, introducing the ideas of the elements and constituents of the matter. Democritus, the great philosopher who was living in the 4th century B.C., said: After certain number of divisions, a limit is reached where the part can not be divided any further; all substances are built from invisible particles, which he called '**atoms**' from the Greek uncuttable, indivisible.

However, a genuinely scientific exploration of the nature has begun in the 17th century with the invention of the necessary instruments. Armed with telescopes, the humanity understood that stars and other twinkling objects seen in the sky represent the visible projection of only a tiny portion of an enormously large Universe populated by billions and billions of galaxies, stars, planets, gaseous nebulas etc. From the other hand, the scientists have initiated the experimental studies of the inner structure of the matter, which finally led to the great discoveries, in the 19th and 20th centuries, of the atoms, nuclei, elementary particles and other constituents of the matter.

However surprising it appears, all the diversity of the Nature is governed and organized by only four forces – carriers of the strong, electromagnetic, weak and gravitational interactions. Three of these forces, strong, electromagnetic, and gravitational, can be called "matter constructing forces", while the weak force is "destructing" the matter. Being of different physical origin, these four forces act on different ranges and have different relative strength (see Table 1.1).

THE FORCES OF THE NATURE		
Interaction type	**Range**	**Strength at 10^{-13} centimeter in comparison with strong interaction force**
Strong	About 10^{-13} cm	1
Electromagnetism	Infinite	10^{-2}
Weak	Less than 10^{-16} cm	10^{-13}
Gravity	Infinite	10^{-38}

Table 1.1 Relative strength and range of action of the four forces of the Nature.

Strong interactions are responsible for interaction between the hadrons (see Chapter 3), binding the neutrons and protons into nuclei. They also confine the elementary constituents of strong interacting matter – quarks and gluons into baryons and mesons (see Chapter 4). The range of strong interaction forces does not extend but to a few 10^{-13} centimeters.

The electromagnetic forces have infinite long range of action. They bind electrons and nuclei to atoms, atoms to molecules and glue molecules to one another to make solids, liquids and gases. The majority of the macroscopic forces, such as friction and elasticity forces, have their origin just in the electromagnetic interactions.

As its name indicates, the weak interaction is weaker than the strong and electromagnetic interactions. It is responsible for radioactivity of the matter and it can change one particle into another, for example a neutron into a proton or a proton into a neutron. The weak force regulates how the Sun burns and supplies the Earth with the energy, the source of life on our planet.

Gravity is the weakest of the four interaction forces. Having very small interaction strength (see Table 1.1) and being dependent proportionally on the mass of the interacting bodies, its effect on the elementary particles is negligible as compared to the other forces. Meanwhile, since it has infinitely long range of action just gravity is gripping planets, stars, galaxies and other large scale cosmic objects and steering their relative movements.

Chapter 2 *Measurement Units Used in Particle Physics*

The size, charge and mass of the subatomic particles are so small that it is very inconvenient to use for their description a standard system of units. Instead, an adequate system of units has been introduced by physicists. This system is described below.

Charge unit

The charge unit, e, is equal to the magnitude of the proton charge, whose values in coulombs is

$$e = 1.602 \times 10^{-19}\ \text{C} \tag{2.1}$$

In this unit, the charge, q_a, of a particle a is given by the equation:

$$q_a = Q_a / e \tag{2.2}$$

where Q_a is the charge of this particle in C. For instance, in the units of e, the electron charge is equal to –1.

Distance unit

The distance unit used in subatomic physics is

fermi (fm): $1\ \text{fm} = 10^{-13}\ \text{cm}$

It is named after the Italian physicist Enrico Fermi (1901–1954)

Time unit

The time unit in particle physics is

second (s)

Energy unit

The natural scale of the energy and work on the microscopic level is given by a unit called

electronvolt (eV)

1 eV is equal to the energy gained by an electron when crossing a gap between two electrodes that are connected to a 1-volt battery. Let us find the relation between 1 eV and 1 joule (J). Since the magnitude of the electron electric charge is equal to (2.1) and 1 J = 1 V × 1 C, this gives

$$1\ \text{eV} = 1e \times 1\text{V} = 1.602 \times 10^{-19}\ \text{J}$$

In high energy particle physics one also uses the multiple units of eV: **kilo–electronvolt** (KeV): 1 KeV = 10^3 eV, **mega–electronvolt** (MeV): 1 MeV = 10^6 eV, **giga–electronvolt** (GeV): 1GeV = 10^9 eV, **tera–electronvolt** (TeV): 1 TeV = 10^{12} eV.

Area unit

The widely used units of area are:

$$\boxed{\text{i) fm}^2 \text{ and ii) } \textbf{barn} \text{ (b): 1 b } = 100 \text{ fm}^2}$$

and the submultiples of barn: **milli–barn** (mb): 1mb = 10^{-3} b, **micro–barn** (μb): 1 μb = 10^{-6} b, **nano–barn (nb)**: 1nb = 10^{-9} b and **pico–barn** (pb): 1 pb = 10^{-12} b.

The units for the 3-dimentional momentum (***p***) and mass (*m*) of a particle are derived from the equation of the special theory of relativity, which connects energy, momentum and mass

$$\boxed{E^2 = \boldsymbol{p}^2 c^2 + m^2 c}$$

where *c* is the speed of the light.
Since both sides of this equation have to have the same dimension, one concludes that:

$$\boxed{\textbf{the momentum unit is eV } c^{-1} \textbf{ and the mass unit is eV } c^{-2}}$$

c=1, ħ=1 and k=1 convention

The formulae of the particle physics represent complex expressions containing numerous symbols. Especially repeatedly appear such symbols as *c*, *ħ* (reduced Planck's constant) and *k* (Boltzman constant).

In order to facilitate the presentation of formulae and to make them more transparent for reading and understanding, the physicists have adopted a convention

$$\boxed{\boldsymbol{c} = 1,\ \boldsymbol{\hbar} = 1,\ \boldsymbol{k} = 1} \qquad (2.3)$$

Apart from making easier the presentation of formulae, this convention leads to the interesting relations between the time, distance, energy and temperature. We will proceed now to their derivation.

The speed of light is expressed through the units of fermi and second as

$$\boxed{c = 299\ 792\ 458 \times 10^{15} \text{ fm s}} \qquad (2.4)$$

The quantum mechanical particle-wave duality is expressed by the connection of the photon energy E to its wavelength λ

$$\boxed{E = 2\pi\hbar c/\lambda} \quad \text{with} \quad \boxed{\hbar = 6.583 \times 10^{-16} \text{ eV s}} \qquad (2.5)$$

Consider now the Boltzman constant *k*.

$$\boxed{k = R/N_A = 8.617 \times 10^{-5} \text{ eV K}^{-1}} \qquad (2.6)$$

where R is the universal gas constant and N_A is the Avogadro number.

One sees from equations (2.4), (2.5) and (2.6) that the convention (2.3) allows to express the units of distance, time, energy and temperature through only one of them. In practice, however, one uses the following units: eV (and its multiples), fm, barn (and its submultiples) and s. We give below some widely used conversion formulae:

From $\hbar c = 1 = 197.327$ MeV fm, one gets that

$$\boxed{1 \text{ MeV} = 5.068 \times 10^{-3} \text{ fm}^{-1} \text{ and } 1\text{mb} = 2.568 \text{ GeV}^{-2}.} \qquad (2.7)$$

From $k = 1$ and (2.6), one gets that.

$$\boxed{1 \text{ eV} = 11605 \text{ K}} \qquad (2.8)$$

In the process of problem solving for a physical quantity, the physicists are usually using convention (2.3). At the end of the work, they revert (using the conversion formulae like (2.7) and (2.8)) to the meaningful for that quantity units.

Chapter 3 *Strong Interactions (SI). Hadrons: Their Properties. Conservation Laws of SI*

As it was said in Chapter 1, the spatial range of SI is restricted to the subnuclear distances less than a few fermis. The SI processes go very fast, at a time of the order of 10^{-23} sec. Let us proceed now to a more detailed description of the characteristics of SI. Hadrons (from Greek '**hadros**' – strong, robust) are the particles that take part in SI. By now about two hundred of hadrons are discovered. A complete list of all known particles, including hadrons, and review of their properties is published each two years by Particle Data Group (PDG). The data used below are taken from the 2004 publication of PDG (Reference 1).

Hadrons posses a series of quantum attributes:

Spin: We assume that the reader is familiar with this quantum intrinsic angular momentum of particle. The hadrons can be divided in two big groups – baryon (from Greek '**barys**' – heavy) group and meson (from Greek '**mesos**'– middle, intermediate) group. All baryons (for instance, neutron and proton) are fermions, i.e. they have half-unit value of spin. The mesons (pion, kaon, etc.) are bosons, i.e. particles with integer spin.

Baryon number: All baryons carry the baryon number *(N_B)* equal to +1.

Flavour number: There exist four flavour numbers: strangeness (S), charm (C), bottomness, or beauty (B) and topness, or truth (T).

Isospin: Isospin is a physical quantity which is mathematically analogous to spin. Isospin was introduced by the German physicist Werner Heisenberg (1901–1976) to explain the fact that the strength of SI is almost the same between two protons or neutrons as between a proton and a neutron, unlike the electromagnetic interactions which depend on the electric charge of the interacting particles. Heisenberg's idea was that protons and neutrons are essentially two states of the same particle, the nucleon with isospin equal 1/2. The proton corresponds to the 'isospin-up' state (that is the +1/2 projection on the third, z–axis in the isospin space) whereas the neutron to the 'isospin-down' state (the –1/2 projection) of the nucleon isospin, which is equal to 1/2. In general, the number of the charge states (projections on the third axis) corresponding to the isospin I is equal to $2I + 1$ and one says that these states constitute $2I + 1$ multiplet of the isospin I. For example, π^+, π^o and π^- –mesons (see below) represent +1, 0 and –1 projections of the isospin 1 carried by the pion. One says also that these pions represent the triplet of isospin 1.

In 1953, theorists Murray Gell-Mann (born in1929) from USA and Kazuhiko Nishijima (born in1926) from Japan had suggested a formula, which connects the electrical charge, defined by (2.2), of strangeness carrying hadron to the projection of the isospin, baryon number and strangeness of this hadron. The generalization of their formula to the case of any flavour reads as

$$q = I_3 + \frac{N_B + S + C + B + T}{2} \qquad (3.1)$$

The hadrons posses also attributes, which are connected to the operations of charge conjugation (***C–conjugation***), combined *C*-conjugation and rotation in the isospin space (***G–operation***) and spatial inversion (***P–inversion***). Let us proceed to the explanation of these operations.

C–conjugation: The replacement of particles by their antiparticles is called the operation of charge (or *C*–) conjugation. *C*–conjugation changes the sign of all attributes of a particle (like electrical charge, magnetic moment, and baryon and flavour numbers), except that of the momentum, spin and isospin. Therefore if a particle a has only the last three attributes, then $\overline{a}$ is its own antiparticle. In that case one speaks about the *C*–parity of the particle a. The neutral pion is such particle. Its *C*–parity is equal +1. If the particle a has an attribute beyond the last three, the antiparticle $\overline{a}$ has the opposite attributes. The examples are neutron (n) and proton (p). In the case of p, the charge obviously distinguishes p from $\overline{p}$, while n, though electrically neutral, carries the baryon number and the magnetic moment that have the opposite sign from that of $\overline{n}$.

G–operation: Let us consider the *C*–conjugation in combination with the rotation in the isospin space by 180^{o} around the second, y-axis. Such rotation will carry the I_3 projection into $-I_3$, converting, for instance, a $\boldsymbol{\pi}^{+}$ into $\boldsymbol{\pi}^{-}$ (and vice versa). If one then applies the charge conjugation, one comes back to $\boldsymbol{\pi}^{+}$.

The unflavoured mesons possess *G*–parity attribute which is given by

$$G = (-1)^{I}C$$

where I is the isospin of the multiplet and C is the *C*–parity of the neutral member of the multiplet. It is important that *G*–parity is an attribute possessed by all the members of the isospin multiplet. In case of pions $I = 1$ and $C = +1$, which gives $G = -1$, so one speaks about the negative *G*–parity of all three pions.

P-inversion: *P*–inversion is the space reflection. Examples are reflection in a plane, say in the x–y plane

$$(x, y, z) \rightarrow (x, y, -z);$$

and reflection through the origin

$$(x, y, z) \rightarrow (-x, -y, -z)$$

Different quantities are transforming differently under *P*–inversion. For instance, polar vectors change their sign, while axial vectors do not. Scalars do not change their sign, but pseudoscalars do. One tells that the polar (axial) vectors have spatial parity, or *P*–parity, equal to –1 (+1). The scalars (pseudoscalars) have *P*–parity equal +1 (–1).

All hadrons have definite value of *P*–parity, which is determined in the experiments, assuming that parity of proton and neutron is positive. For instance, the π-mesons triplet has negative *P*–parity.

Besides, SI are invariant under the operation of time (*T*–) reversal The invariance of the strong interaction under *T*–reversal leads to definite relations between direct (say, $a + b \rightarrow c + d$) and reverse ($c + d \rightarrow a + b$) reactions.

Combination of *T*–reversal, *C*–conjugation and *P*–inversion is called *TCP*–operation. There exists a famous *TCP* theorem that states that the *TCP*–operation is an exact symmetry of any interaction. *TCP* theorem has a few fundamental consequences for the elementary particle physics. The requirement that the particles and their antiparticles should have equal masses and lifetimes is among them.

The quantum numbers of flavour, baryon and charge are additive numbers, i. e., for a system of particles these numbers represent the algebraic sum of the corresponding quantum numbers of constituents. The *C–, P–, T* – and *G* –parities of a system represent the product of the parities of the constituents, i. e. these parities are the multiplicative quantities. Both spin and isospin add-up quantum mechanically. For instance, spin J of a system of two particles with spins J_1 and J_2, runs the numbers $|J_1 - J_2|$, $|J_1 - J_2 + 1|$, ……, $J_1 + J_2$.

Let us consider in more detail the group of baryons. These half-unit spin hadrons are distinguished by the following attributes: ***flavour number, spin (J), isospin (I)*** and ***P–parity (P)*** **.** In Table 3.1 we list the main properties of experimentally established baryons with baryon number $N_B = +1$, classified in accordance with the Reference 1.

N– and Δ–baryons (uflavoured baryons with $I = 1/2$ and 3/2)
Ground states**:** $p(1/2^+, 938.27\ \text{MeV}, \infty)$ and $n(1/2^+, 939.56\ \text{MeV}, 14\ \text{min}\ 45.7\ \text{s})$
Resonances**:** 13 I=1/2 baryons from $N(1/2^+, 1440\ \text{MeV})$ to $N(11/2^-, 2600\ \text{MeV})$ and 10 I=3/2 baryons from $\Delta(3/2^+, 1232\ \text{MeV})$ to $\Delta(11/2^+, 2420\ \text{MeV})$
Λ–baryons (baryons with strangeness $S = -1$ and $I = 0$)
Ground states**:** $\Lambda(1/2^+, 1115\ \text{MeV}, 2.6\times10^{-10}\ \text{s})$
Resonances**:** 13 baryons from $\Lambda(1/2^-, 1405\ \text{MeV})$ to $\Lambda(9/2^+, 2350\ \text{MeV})$
Σ–baryons (baryons with strangeness $S = -1$ and $I = 1$)
Ground states**:** $\Sigma^+(1/2^+, 1189\ \text{MeV}, 0.8\times10^{-10}\ \text{s})$, $\Sigma^0(1/2^+, 1192\ \text{MeV}, 7.4\times10^{-20}\ \text{s})$ and $\Sigma^-(1/2^+, 1197\ \text{MeV}, 1.4\times10^{-10}\ \text{s})$
Resonances**:** 9 baryons from $\Sigma(3/2^+, 1385\ \text{MeV})$ to $\Sigma(?^?, 2250\ \text{MeV})$
Ξ–baryons (baryons with strangeness $S = -2$ and $I = 1/2$)
Ground states**:** $\Xi^0(1/2^+, 1314\ \text{MeV}, 2.9\times10^{-10}\ \text{s})$ and $\Xi^-(1/2^+, 1321\ \text{MeV}, 1.6\times10^{-10}\ \text{s})$
Resonances: 5 baryons from $\Xi(3/2^+, 1530\ \text{MeV})$ to $\Xi(\geq5/2^+, 2030\ \text{MeV})$
Ω–baryons (baryons with strangeness $S = -3$ and $I = 0$)
Ground states: $\Omega^-(3/2^+, 1672\ \text{MeV}, 0.8\times10^{-10}\ \text{s})$
Resonances*:* One baryon – $\Omega^-(?^?, 2250\ \text{MeV})$
Λ_c, Σ_c, Ξ_c, Ω_c–baryons (baryons with charm $C = +1$)
The principal feature distinguishing the baryons of this ensemble from Λ–, Σ–, Ξ– and Ω–baryons is the replacement in the last baryons of the strangeness $S = -1$ quantum number by the charm $C = +1$ quantum number. The symbol Λ_c is to label baryons with $I = 0$ and $C = +1$, in analogy with $I = 0$ and $S = -1$ baryons. The symbol Σ_c is used for baryons with $I = 1$ and $C = +1$, etc.
Ground states**:** $\Lambda_c^+(1/2^+, 2284\ \text{MeV}, 2\times10^{-13}\ \text{s})$, $\Xi_c^+(1/2^+, 2466\ \text{MeV}, 4.42\times10^{-13}\ \text{s})$, $\Xi_c^0(1/2^+, 2471\ \text{MeV}, 1.12\times10^{-13}\ \text{s})$, $\Omega_c^0(1/2^+, 2697\ \text{MeV}, 0.69\times10^{-13}\ \text{s})$
Resonances**:** In Reference 1 one finds in all 9 established baryons belonging to this ensemble from $\Lambda_c(1/2^-, 2593\ \text{MeV})^+$ to $\Xi_c(3/2^-, 2815\ \text{MeV})$
Λ_b–baryons (baryons with bottomness $B = -1$)
The symbol Λ_b is to label baryons with $I = 0$ and $B = +1$, in analogy with $I = 0$ and $S = -1$ baryons.
Ground states**:** Reference 1 notes only one $I = 0$ $\Lambda_b^0(1/2^+, 5624\ \text{MeV}, 1.229\times10^{-12}\ \text{s})$ baryon. Its isospin, 0, spin, 1/2, and positive P–parity are the theoretical predictions.

Table 3.1 Baryon group of hadrons. The ground states refer to the lightest baryons in the sectors with given flavour number. The notation for a ground state a is $a(J^P, m, \tau)$ with J = spin, P = P-parity, m = mass and τ = lifetime and the notation for resonances is $a(J^P, m)$. All ground states decay via either weak or electromagnetic interactions. The resonances are baryons that decay via SI. The question-mark for an attribute means that this attribute is not yet established in the experiment.

Table 3.1 lists baryons. Evidently, there should also be existing the charge conjugate states of all these baryons, called antibaryons. Some attributes of antibaryon $\bar{a}$ coincide with those of baryon a, the others have opposite sign. All antibaryons have baryon number $N_B = -1$. The energy, momentum, spin, isospin are the same for a and $\bar{a}$, while the electrical charge, flavour

number, third projection of isospin, magnetic moment and *P*–parity differ by sign. By now only a few antibaryons are observed experimentally. The antiproton and antineutron are among them.

Let us proceed now to the group of mesons. Mesons are classified/distinguished by the following attributes: ***flavour number, spin (J), isospin (I)***, ***P–parity, C-parity and G-parity.*** The last two attributes have definite values only for the unflavoured mesons. Reference 1 is giving the following classification of mesons.

Unflavoured mesons ($S = C = B = 0$)
***Ground states*:** $\pi^{\pm}(1^-(0^-)$, 139.57 MeV, 2.6 10^{-8} s) and $\pi^0(1^-(0^{-+})$, 134.98 MeV, 8.4× 10^{-17} s)
***Resonances*:** 65 mesons from $\eta(0^+(0^{-+})$, 547.75 MeV) to $\Upsilon(0^-(1^{--})$, 11.019 GeV)
Strange mesons ($S = \pm 1$, $C = B = 0$)
***Ground states*:** $K^{\pm}(1/2\ (0^-)$, 493 MeV, 1.2 $\times 10^{-8}$ s), $K_S^0(1/2\ (0^-)$, 0.89 $\times 10^{-10}$ s) and $K_L^0(1/2\ (0^-)$, 5.18 $\times 10^{-8}$ s) (see also the text)
Resonances: 11 mesons from $K^*(1/2\ (1^-)$, 892 MeV) to $K_4^*(1/2(4^+)$, 2045 MeV)
Charmed mesons ($C = \pm 1$)
***Ground states*:** $D^{\pm}(1/2(0^-)$, 1869 MeV, 1.04 $\times 10^{-12}$ s) and $D^0(1/2(0^-)$, 1864 MeV, 4.1$\times 10^{-13}$ s)
Resonances: 5 mesons from $D^*(1/2(1^-)$, 2007 MeV) to $D_2^*(1/2(2^+)$, 2460 MeV)
Charmed, strange mesons ($C = S = \pm 1$)
***Ground states*:** $D_s^{\pm}(0(0^-)$, 1968 MeV, 4.90 $\times 10^{-13}$ s)
***Resonances*:** 5 mesons from $D_s^{*\pm}(0(?^?)$, 2112 MeV) to $D_{s2}(0(?^?)$, 2572 MeV)
Bottom mesons ($B = \pm 1$)
***Ground states*:** $B^{\pm}(1/2(0^-)$, 5279 MeV, 1.67 $\times 10^{-12}$ s) and $B^0(1/2(0^-)$, 5279 MeV, 1.5$\times 10^{-15}$ s)
Resonances: One meson $B^*(1/2(1^-)$, 5325 MeV)
Bottom, strange mesons ($B = \pm 1$, $S = \mp 1$)
***Ground states*:** $B_s^0(0(0^-)$, 5369 MeV, 1.46 $\times 10^{-12}$ s)
Bottom, charmed mesons ($B = C = \pm 1$)
***Ground states*:** $B_c^{\pm}(0(0^-)$, 6.4 GeV, 0.46× 10^{-12} s)

Table 3.2 Meson group of hadrons. The ground states refer to the lightest mesons in the sectors with given flavour numbers. The notation for unflavoured ground states is $a(I^G, J^{PC}, m, \tau)$ with I = isospin, G = G–parity, J = spin, P = P–parity, C = C–parity, m = mass and τ = lifetime and the notation for the resonance unflavoured states is $a(I^G, J^P, m)$. The notation for ground flavoured states is $a(I, J^P, m, \tau)$ and that for flavoured resonances is $a(I, J^P, m)$. All ground states decay via either weak or electromagnetic interactions. The resonances are mesons that decay via SI. The question-mark for an attribute means that this attribute is not yet established in the experiment.

As distinct from the case of baryons, Table 3.2 includes both mesons and antimesons. For instance, the π –meson triplet is represented by π^+ and π^-, which are antiparticles to each other, and π^0 which is identical to its antiparticle.

The case of neutral $S = \pm 1$ lightest mesons requires a special explanation. The states with definite value of strangeness are $K^0(S = +1)$ and $\overline{K}^0(S = -1)$ mesons. However, the particles one normally observes in laboratory are not K^0 and $\overline{K}^0$, but other two, $K_S^0(1/2\ (0^-)$, 0.89 $\times 10^{-10}$ s)– and $K_L^0(1/2\ (0^-)$, 5.18 $\times 10^{-8}$ s)–mesons. The interpretation of this phenomena in the language of the quantum mechanics is that the states K_S^0 and K_L^0 represent linear

combinations of the states K^0 and $\overline{K}^0$. Being mixtures of the states with $S = +1$ and $S = -1$, K_S^0– and K_L^0–mesons have no definite value of strangeness.

Typical size of hadrons and their lifetime.

Typical size of hadrons is of the order of 1fm. All hadrons except proton are unstable, that is they decay into other particles. The most long-living among unstable hadrons is the neutron which decays via weak interactions into proton, electron and electron antineutrino (this is called beta decay of neutron). The lifetime of neutron is 14 min 45.7 sec. The other hadrons have much shorter lifetimes. Dispersed over large interval from 10^{-8} up to 10^{-24} sec, these lifetimes reveal the following regularities. For unflavoured sets of baryons and mesons, as well as for sets with given flavour, the lifetimes of lightest, ground states are occupying an interval from 10^{-8} to 10^{-14} sec. Exception constitute long-living neutron (see above), as well as π^0–meson and Σ^0–baryon, whose lifetimes are 8.4×10^{-17} s and 7.4×10^{-20} s, respectively. Higher lying meson and baryon resonances have lifetimes less than 10^{-23} sec. The relatively large lifetime of the ground states is due to their decay through the weak interaction processes, which do not conserve either isospin or flavour. The very long lifetime of the neutron, which also decays through the weak interactions, is caused by a very small energy release in its decay. The 'exceptionally short' lifetimes of π^0 and Σ^0 ground states is explained by their decay through the electromagnetic interaction, which is much more intensive than the weak one. Finally, the very short lifetime of the resonances is caused by their decay through SI.

Conservation laws of SI

SI are subject to various conservation laws, which are very helpful in the analysis and systematization of these interactions. For the processes involving hadrons, the number of conserving quantities and invariances is maximal for SI and minimal for the weak interactions (see Table 3.3).

Conservation laws of SI	***Electromagnetic interaction of hadrons***	***Weak interaction of hadrons***
Energy-momentum	*yes*	*yes*
Total angular momentum	*yes*	*yes*
Electric charge	*yes*	*yes*
Baryon number	*yes*	*yes*
Isospin	*no*	*no*
Flavour number	*yes*	*no*
C–invariance	*yes*	*no*
G–invariance	*no*	*no*
P–invariance	*yes*	*no*
T–invariance	*yes*	*no*
TCP–invariance	*yes*	*yes*

Table 3.3 Conservation laws of SI and their validity in the electromagnetic and weak interactions.

Chapter 4 *Quarks and Gluons as Elementary Constituents of Strongly Interacting Matter*

The powerful electron–proton, electron–positron, proton–proton and antiproton–proton accelerators created in the second half of the last century allowed to discover and study quarks, the elementary constituents of the hadronic matter. The word *quark* was introduced by Gell–Mann. Its origin is an enigmatic quotation from James Joyce's *Finnegans Wake* – 'three quarks for Muster Mark'). Six quarks are discovered until now: up, down, strange, charmed, bottom and top. The quantum numbers/attributes and masses of these quarks are given in Table 4.1. The charge of quarks is determined by Eq. (3.1).

Name	Symbol	Electrical charge	Isospin	Mass *)	Flavour number
Up	***u***	+2/3	1/2	1.5 to 4 MeV	-
Down	***d***	–1/3	1/2	4 to 8 MeV	-
Strange	***s***	–1/3	0	80 to 130 MeV	*Strangeness* = –1
Charmed	***c***	+2/3	0	1.15 to 1.35 GeV	*Charm* = +1
Bottom	***b***	–1/3	0	4.1 to 4.4 GeV	*Bottomness* = –1
Top	***t***	+2/3	0	174.3±5.1 GeV	*Topness* = +1
All quarks have baryon number 1/3, spin 1/2 and positive P–parity					
For antiquarks, the baryon number, electrical charge, P–parity, third projection of isospin and flavour number have the sign opposite to that of quarks					
*) The values of masses are taken from Reference 1					

Table 4.1 Characteristics of quarks.

All these six quarks posses an additional quantum number, called colour. The colour has three components, which are traditionally denoted by red, green and blue. Each quark can be in any of these three colour states. Due to their colour 'charge', quarks are interacting with each other by means of eight mesons called gluons (derivative of 'glue'). The gluons are also carrying the colour and so they are also interacting with each other (this is called the selfinteraction of gluons). The theory which describes the interaction of quarks and gluons is called Quantum Chromodynamics (QCD). Gluons have no masses, their spin is equal 1 and *P*–parity is –1 and they do not carry electrical charge, isospin and any flavour number. At first glance, the gluons seem to be very similar to photons, which carry the electromagnetic interaction between the electrically charged particles and one could think about similarity of QCD and Quantum Electrodynamics (QED), the quantum theory of the electromagnetic interactions. Indeed, at small distances between the quarks and gluons their interaction can be described by the Coulomb–like potential, with very small interaction constant, quite as the interaction between the electrically charged particles in QED. This situation is called 'ultraviolet, or asymptotic freedom' of QCD. However, at large distances the behaviour of the colour interaction potential differs drastically from the electric one. The electric interaction potential continues to follow the $1/r$ law (where r is the distance between the electrical charges), while the chromoelectric interaction potential changes its behaviour and becomes growing linearly with the distance between the quarks and antiquarks. This peculiar behaviour of the chromoelectric forces at large distances is due to the intensive selfinteraction of gluons. This is the origin of the difference between QCD and QED since the photons are electrically neutral and interact very weakly with each other.

The linear increase of the chromoelectric interactions potential at large distances leads to the so-called confinement of quarks and gluons, which means that neither quarks nor gluons can exist as free states and they are necessarily confined to the colourless hadrons.

Figure 4.1 demonstrates the difference between: **a)** electric and **b)** chromoelectric fields at large separation of the opposite electric and colour charges.

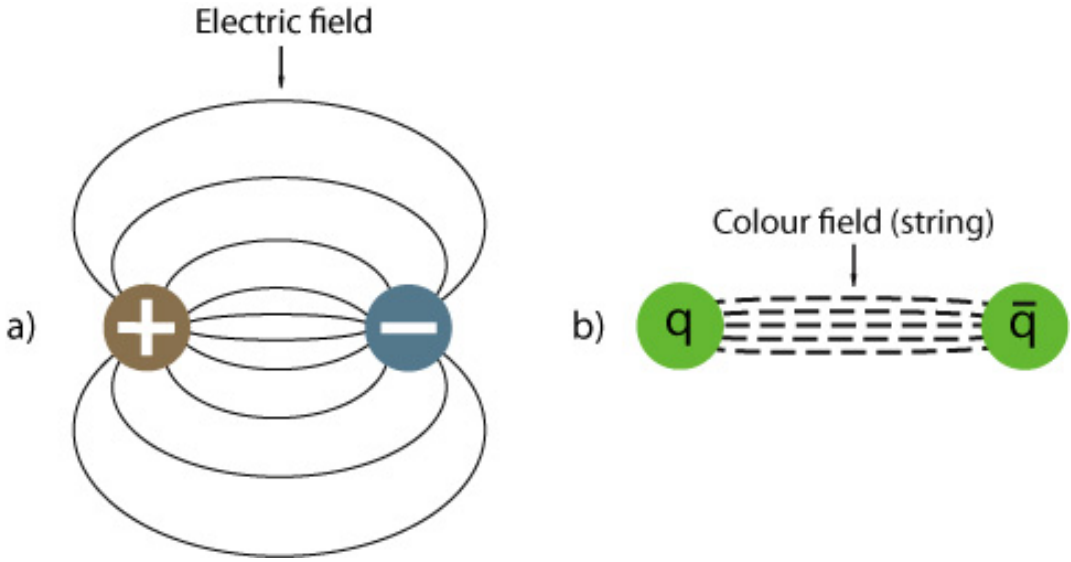

Figure 4.1 a) Electric field surrounding two opposite charges and **b)** Colour field of a $q\bar{q}$ pair. In contrast to QED, where the lines of force can spread in the all space, in QCD the lines of force are compressed into a 'flux tube' (or a 'string'), as if there were an attraction between the line of forces.

The effect of confinement is demonstrated in Figure 4.2. As we stretch the string between the quark and antiquark (Fig 4.2a), it becomes energetically favourable to create a quark pair by the string fission (Fig 4.2b), which then results in the transition from a one– to a two– $q\bar{q}$ state (Fig 4.2c).

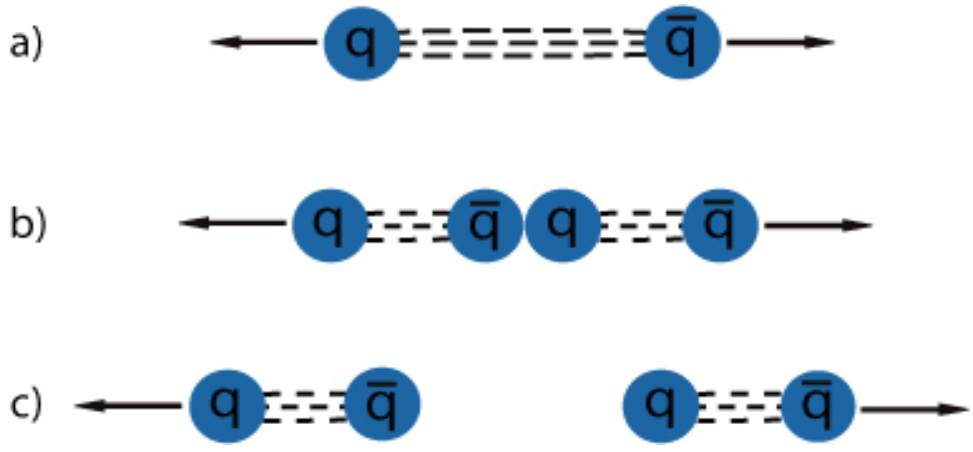

Figure 4.2 Scenario for quark confinement at large spatial separation between the quark and antiquark.

The described in the Chapter 3 mesonic and baryonic states of hadrons find their classification within the quark model and QCD. So, meson is represented as colourless state containing symmetric over colours combination of three pairs of valence quark-antiquark tied by

the colour string. The valence quarks carry together the quantum attributes of meson. Figure 4.3a shows one of the three colour-anticolour components of meson.

Baryon is constructed as colourless state containing the antisymmetric over colours combination of three valence quarks, which carry together the quantum attributes of the baryon. The quarks in baryon are tied to each other by the three colour strings/tubes, which converge to a common vertex called string junction. Figure 4.2b shows one of the six colour configurations of three valence quark components of a baryon.

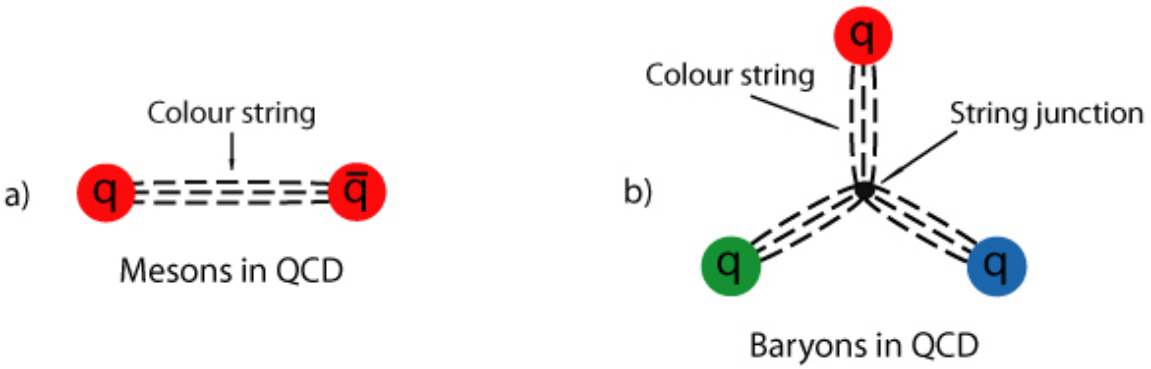

Figure 4.3 a) The red-antired quark component of a meson. The colourless meson contains also blue-antiblue and green-antigreen components. **b)** One of the six colour configurations of three quarks making up together a colourless baryon.

In Table 4.2 we present the quark content of the lightest, for given flavour and isospin, baryons and mesons.

Baryons	***Quark content***	**Mesons**	***Quark content***
p	uud	$\pi^+, \pi^- \ \pi^o$	$u\bar{d}\ ,\ d\bar{u}\ ,\ (u\bar{u}+d\bar{d}\ )/\sqrt{2}$
n	udd	$K^+, K^-,\ K^0,\ \overline{K}^0$	$u\bar{s}\ ,\ \bar{u}s\ ,\ d\bar{s}\ ,\ \bar{d}s$
$\Delta^{++}, \Delta^+, \Delta^0, \Delta^-$	$uuu,\ uud, udd,\ ddd$	$D^+, D^-, D^0, \overline{D}^0$	$c\bar{d}\ ,\ \bar{c}d\ ,\ c\bar{u}\ ,\ \bar{c}u$
Λ^o	uds	$D_S^+,\ D_S^-$	$c\bar{s}\ ,\ \bar{c}s$
$\Sigma^+, \Sigma^0, \Sigma^-$	$uus,\ uds,\ dds$	$B^+, B^-,\ B^0,\ \overline{B}^0$	$u\bar{b}\ ,\ \bar{u}b\ ,\ d\bar{b}\ ,\ \bar{d}b$
Ξ^0, Ξ^-	$uss,\ dss$	$B_S^0,\ \overline{B}_S^0$	$s\bar{b}\ ,\ \bar{s}b$
Ω^-	sss	$B_C^+,\ B_C^-$	$c\bar{b}\ ,\ \bar{c}b$
$\Lambda_C^+,\ \Sigma_C^{++},\ \Sigma_C^+,\ \Sigma_C^0,$ $\Xi_C^+,\ \Xi_C^0,\ \Omega_C^0$	$udc,\ uuc,\ udc,\ ddc,$ $usc,\ dsc,\ ssc$		
$\Lambda_b^0,\ \Xi_b^0,\ \Xi_b^-$	$udb,\ usb,\ dsb$		

Table 4.2. Valence quark structure of lightest, for given flavour and isospin, baryons and mesons.

Chapter 5 *A New, Extremely Dense and Hot State of Matter – Quark-Gluon Plasma (QGP)*

At not too high temperature T (T ≤ 1 eV = 11605 K, see Eq. (2.8)), the matter is classified by three aggregate states: gaseous, liquid and solid states, representing ensembles of the molecules and atoms. At temperatures higher than binding energies of the electrons inside the atoms, the matter converts to a state of the free electrons and ions, called electromagnetic plasma (EP). There exist different types of EP covering a temperature interval from 10^5 to 10^9 K, i.e. an energy interval from 10 eV to 100 KeV. The overwhelming quantity of the actual Universe matter is in the EP state: stars, star atmospheres, galactic nebulae and interstellar medium. One finds the EP near the Earth also, in the way of the solar wind.

At temperatures above the binding energies that keep the nucleons inside the atomic nuclei (a few MeV), the nuclei dissociate into neutrons and protons, accompanied by other hadrons (π, K and other mesons, strange baryons and baryon resonances). One speaks in this case about an aggregate state (gaseous or liquid) of the hadron matter. Ultimately, there are theoretical expectations that at temperatures above 150÷200 MeV (more than 10^{12} K), the hadron matter can not be more considered as an ensemble of the individual hadrons. At these temperatures quarks and gluons are no longer confined within hadrons and create a deconfined type of matter called Quark-Gluon Plasma (QGP). It is expected that at the very early stages of

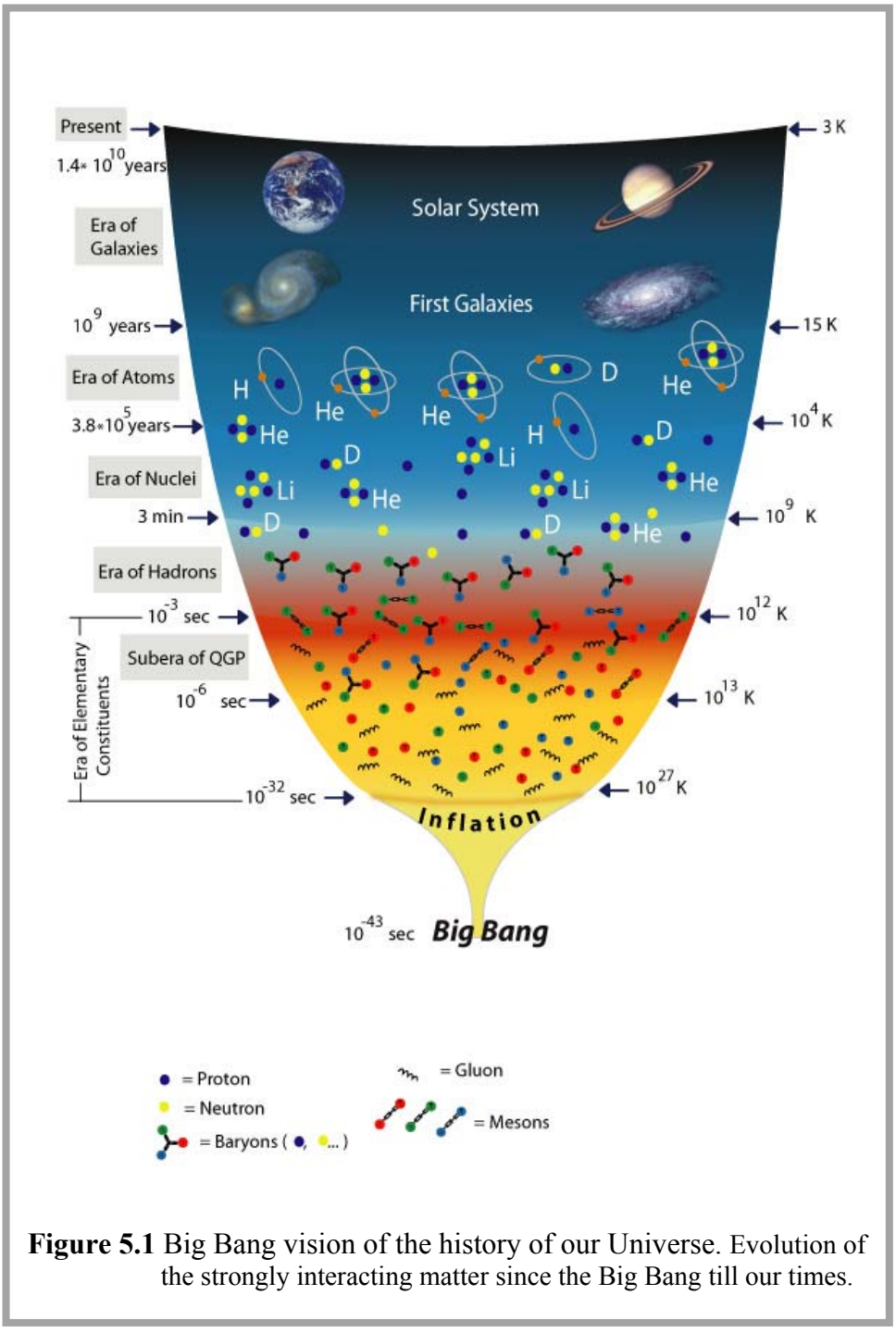

Figure 5.1 Big Bang vision of the history of our Universe. Evolution of the strongly interacting matter since the Big Bang till our times.

its evolution the matter of Universe was in the form of QGP.

The widely accepted modern view of the origin and history of the Universe is based on the Big Bang hypothesis. According to this hypothesis, our Universe was born about 14 billion years ago in a big explosion, followed by a rapid inflation, which liberated a huge amount of energy and elementary constituents of the matter. As the Universe expanded and cooled, the particles that make up ordinary matter appeared and formed the structures we see in the Universe today, from atoms to galaxies.

During the 20^{th} century, strong evidences in favour of the Big Bang theory have been accumulated. Among them are the abundances of the light nuclei and the observation of the relic 3–degree microwave background radiation.

The Universe evolution diagram is shown in the Figure 5.1. After initial explosion at Planckian time of 10^{-43} s and extremely rapid inflation till 10^{-32} s, the Universe passed, at a temperature of ~ 10^{26} K and density of ~ 10^{70} gm/cm^3, to the era of the elementary constituents of the matter. The Universe was filled then with the carriers of the weak interactions, *W*– and *Z*–bosons, photons, neutrinos, leptons (not shown in the Figure) as well as with quarks and gluons. In the course of an extremely rapid expansion, different components of this 'soup' were evolving differently and close to the time of about 1 microsecond the Universe entered the QGP phase where the matter component was dominated by quarks and gluons. During the next 1000 microseconds, the QGP cooled under expansion down to the temperature of the order of 10^{12} K and density of the order of 10^{11} gm/cm^3. Due to confinement, the QGP was fully 'frozen' within these 1000 microseconds to the protons, neutrons and other hadrons and the Universe entered the era of hadrons. It took then about 3 min in order all hadrons but neutrons and protons disappear, and the neutrons and protons combine to nuclei of the light elements (D, He, Li….). The evolution of the Universe during the period from this 3–minute age till the time of 380000 years ended by the capture of electrons by nuclei and formation of atoms. These two and next stages of the Universe history are also depicted in Figure 5.1.

Today, quarks and gluons remain locked inside protons and neutrons constituting the ordinary matter. However, matter similar to QGP may still exist at the heart of neutron stars, where the density is so high (see Chapter 7) that a pinhead would contain as much matter as the Great Pyramid of Egypt. At these densities, the distances between the quarks and gluons become very small and due to the ultraviolet freedom, an aggregate state of (almost) free quarks and gluons, i.e. QGP, may be formed.

The discovery of QGP in the laboratory experiments is a great challenge of the modern physics. The details of the experimental approaches to the search for QGP will be described in Chapter 7.

Chapter 6 *Particle and Ion Accelerators as Tools for Laboratory Study of SI*

The properties of SI and hadrons are studied in the World labs with the help of the 'probes' – the beams of particles accelerated until almost the speed of light. These are the beams of directly accelerated electrons and positrons, protons and antiprotons, various ions, as well as the so-called secondary beams of other particles (see below). Higher is the energy of the beams, finer is the structure of the matter that one can investigate using these beams. The overwhelming majority of hadrons was found just in the experiments which were operating with the accelerated in the laboratory beams.

Two kinds of accelerators are constructed and exploited worldwide - fixed target machines and colliders. In fixed target machines, an accelerated particle beam hits an immovable target. In collider mode, the accelerated beams fly in the opposite directions and collide at certain points of the acceleration path. Each of these two modes has advantages and disadvantages. For instance, fixed target machines allow formation of the secondary beams consisting of the particles produced in the interactions of the main beams with the targets. One succeeds to get in this way

the secondary beams of photons, antiprotons, positrons, charged pions and kaons as well as $\Sigma^{\pm}$-hyperons, for the subsequent experiments with these beams. Further, the fixed target mode allows exploitation of a large variety of targets, from hydrogen to the uranium. In their turn, colliders are very useful for the exploration of the physics requiring large available energy. For instance, a 1000–GeV proton bombarding a hydrogen target, can not produce a particle with mass more than 42 GeV while two colliding 1000–GeV proton beams provide an available energy of almost 2000 GeV. Table 6.1 lists some most large world accelerators. All of them but LHC are running at present while the commissioning of LHC is foreseen for the middle of 2007.

There are many accelerator complexes operating in Europe, North and South Americas, China and Japan. Some of them are well known to even grand public by their outstanding role in the investigation of the subatomic physics phenomena. So, the Stanford Linear Accelerator Center (SLAC) in USA is famous by the discovery of the parton/quark structure of protons in a series of the so–called deep inelastic electron–proton scattering experiments performed during the late 1960s and early 1970s. The discovery of the J/Ψ–meson at SLAC and Brookhaven National Laboratory (BNL) in November 1974 was called November Revolution since it proved the existence of a new quark, called 'charm'.

The biggest in the world European research centre, CERN (European Laboratory for Fundamental Physics), comprises a large complex of accelerators designed for speeding up the particles to very different energies – from a few MeV to a few TeV. The discovery, in 1984, of the *W*– and *Z*–bosons by UA1 and UA2 experiments at the proton–antiproton collider is a major CERN success story. Actually the efforts of CERN are concentrated on the construction of a biggest accelerator ever built, the Large Hadron Collider (LHC). The main aim of LHC is the search for a very heavy (with mass of up to 1 TeV) scalar particle, called Higgs boson, in the proton-proton collisions at 7 TeV per colliding proton. According to the modern vision of the subatomic world, the elementary constituents of the matter (as electron, muon, quarks, *W*– and *Z*–bosons) acquired their masses in the interaction with the Higgs boson.

The other accelerator centres, less famous, but not less important have been contributing to the scrupulous measurement of the important physical constants and characteristics of elementary particles, by high-precision checks of the symmetry properties of fundamental interactions.

During the last decade, special attention has been paid to the heavy ion experiments aimed at the search for QGP and study of its properties. At present, the world heavy ion programme consists in numerous experiments running in a large collision energy interval from a few GeV per nucleon up to the SPS and RHIC energies (see Table 6.1). Meanwhile the physical society

High -Energy Accelerators of Particles and Ions			
Accelerator	**Mode**	**Beam particles**	**Beam energy**
PEP (Positron-Electron Project) - **II** SLAC, Stanford, USA	Collider	e^+ - e^-	3.1 × 9 GeV
Tevatron FNAL, USA	Collider	$\overline{p}$ - p	980 × 980 GeV
SPS (Super Proton Synchrotron) CERN, Switzerland	Fixed target	p	up to 450 GeV
		ions	up to 158 GeV per nucleon
RHIC (Relativistic Heavy Ion Collider) BNL, USA	Collider	p - p	100 ×100 GeV
		ion-ion	100 × 100 GeV per nucleon
LHC (Large Hadron Collider) CERN, Switzerland	Collider	p - p	7 × 7 TeV
		ion-ion	2.75 × 2.75 TeV per nucleon

Table 6.1 Main characteristics of the biggest accelerators

anticipates the commissioning in 2007 of the ALICE (A Large Ion Collider Experiment) detector being under construction for the experiments at LHC. The ALICE will investigate head–on collisions of two lead beams accelerated to 2.75 TeV per nucleon, i.e. each ion of lead will carry an energy of 2.75 × 208 (atomic number of the lead) = 572 TeV!

Chapter 7 *Search for QGP in Ultra-Relativistic Heavy Ion Collision Experiments*

The diagram shown in Figure 7.1 demonstrates the phases of the strongly interacting matter at different temperatures and net baryon number densities. The blue strip passes by the boundary between the hadron and QGP phases. It is seen from this diagram that QGP may exists at very different temperatures and baryon densities, So, the mentioned in the Chapter 5 QGP state in the core of the neutron stars is formed at very high baryonic densities and very low temperatures. From the other side, the QGP phase of the early Universe represents an aggregate state of the unbound quarks and gluons at zero net baryon density and very high temperature. The arrow on the middle line in Figure 7.1 follows the scenario for a 'Little Bang' creation in the ultrarelativistic heavy ion collision. Ions, which contain an ordinary baryonic matter at density ρ_0 and very low temperature, collide with each other and produce a hot and dense strongly interacting matter. Faster is the relative movement of the ions, higher is the temperature of this matter. The peak value on the curve corresponds to the collisions at very high energies where one anticipates the formation of QGP. Further turn-down of the curve follows the pattern of the QGP cooling under expansion and transition to the hadronic phase.

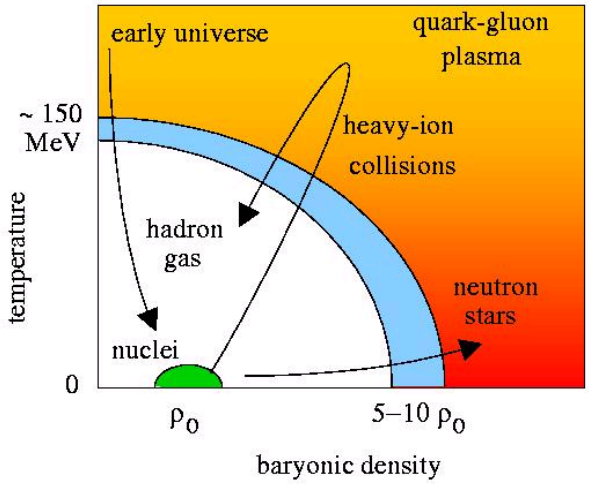

Figure 7.1 Temperature–baryonic density phase diagram of strongly interacting matter

A common believe is that an abundant release of energy and matter in the central collisions of the heavy ions at the LHC would provide the densities and temperatures necessary for the formation of QGP. Together with this, one expects that QGP might be formed even at lower energies of RHIC and SPS and the main difficulty in the proof of the QGP creation at these energies is circumvented by ambiguities in the theoretical treatment of the experimental data.

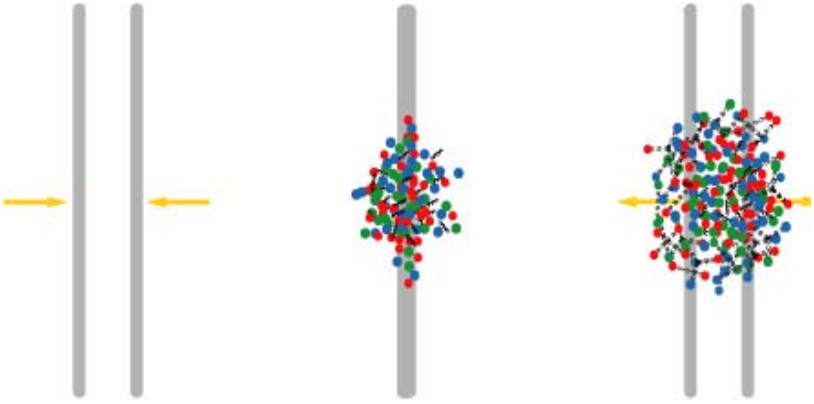

Figure 7.2 Computer simulation of the central collision of the ultrarelativistic heavy ions

Figure 7.2 shows computer representation of a process of the collision of two heavy nuclei moving at almost speed of light. According to

Einstein's theory of special relativity these nuclei look in the laboratory frame like thin pancakes. The 'Little Bang' creates QGP in the laboratory. The QGP expands like a fireball, cools down and finally transforms into ordinary hadronic matter.

Thousands of particles are produced. They have to be recorded by the detectors and the tracks that these particles leave in the detectors have to be analysed by modern powerful software tools. Figure 7.3 demonstrates some of the signals that are produced at different stages of the collision process and have to be registered properly in the experiments. The electromagnetic signals, such as photons, electrons and muons, are produced at every stage of the process and interact weakly with the surrounding matter. The mesons composed of heavy quark-antiquark pairs $c\bar{c}$ and $b\bar{b}$, such as J/ψ and Υ mesons, are produced at the early stages of the collision process. This means that the electromagnetic signals and heavy mesons carry the information about the matter evolution history, which can be studied analysing the properties of the observed signals. Hadrons composed of the light, *u*–, *d*– and *s*–quarks are produced and emitted at the last stages of the evolution process and their study can supply us with the bulk properties of the hadronic phase as well as with the pattern of the QGP freezeout into hadrons.

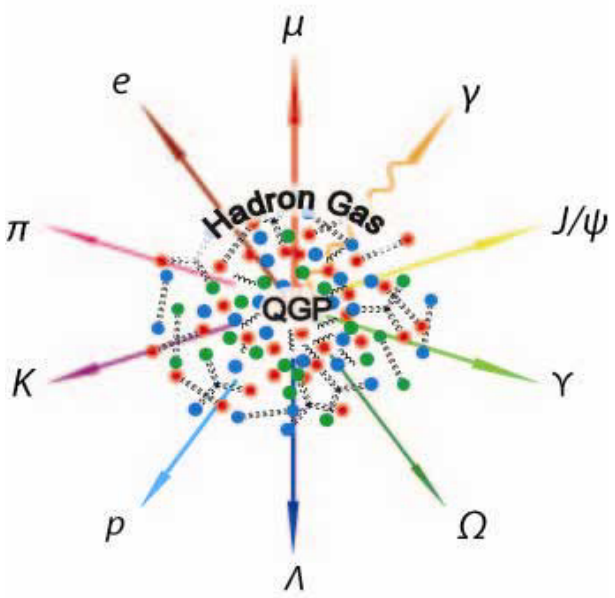

Figure 7.3 Signals–observables emitted by the matter formed in the heavy–ion collisions

In order to distinguish properly the QGP stage from the whole evolution history of the heavy ion collision, an unambiguous analysis of special signals-signatures of the QGP is needed. These signatures are: emission of very energetic (hard) thermal photons, enhanced yield of strange hadrons, fluctuations of the particle multiplicity, J/ψ-suppression, etc. For instance, the production of J/ψ is expected to be suppressed in the hot and dense QGP state as compared to its production in ordinary cold matter. In Chapter 9 we will show how the data of the one of the CERN heavy ion experiments, called NA60, are analysed with the purposes to search for the dynamical fluctuations of the charged particles' multiplicity over the azimuthal angle.

Chapter 8. *Particle Detectors*

In this section, the main particle detectors used in high energy physics are briefly reviewed. Some of these detectors are applied in NA60 experiment at the CERN.

In general, the performance of particle detectors is based on the registration of energy losses of the particle during its passage through the matter of the detector. For example, a charged particle spends a fraction of its energy on ionization and excitation of atoms (molecules).

In **Scintillation detectors**, these losses lead to the emission of photons which can be detected by a photomultiplier, resulting in formation of an electrical impulse. The latter can be coded and recorded in a storing device and used for further analysis.

In **Proportional chambers** or **Multiwire chambers** (filled by a gas mixture of special properties), the primary ionization electrons are accelerated in the internal electrical field created by high-voltage anode wires (stretched in the chamber volume). These accelerated electrons produce a large number of secondary ionization electrons. The latter induce an electrical signal on the anode wire closest to the particle trajectory. Several sets of multiwire proportional chambers allow to reconstruct the particle trajectory. The modern developments of multiwire chambers provide multiple measurement of ionization losses along the particle trajectory. Combined with the measurement of the particle momentum in the magnetic field, these measurements allow to identify what kind of charged particle (electron, muon, pion, kaon, proton) has passed through the chamber.

In **Semiconductor (silicon) detectors**, the energy losses of a particle lead to liberation of electrical charge which is collected (under influence of an external electrical field) on electrodes, resulting in formation of an electrical impulse. Usually silicon detectors consist of a large number of segments (pixels or strips) of the size about 50-200 μm, which provide a high-precision measurement of particle coordinates and the reconstruction of its trajectory.

Transition radiation detectors utilize the effect of x-ray radiation by a high-energy charged particle crossing the boundary between vacuum and a medium. The intensity of the transition radiation increases with the particle Lorentz-factor $\gamma = E/m$, which allows to disentangle a low-mass particle (an electron having large γ) from a heavier-mass particle (e.g. pion having smaller γ).

Cherenkov detectors utilize the effect of Cherenkov radiation – the light emission by a charged particle the velocity v of which exceeds the light velocity c/n in the medium of refractive index n. Usually the Cherenkov detectors with gas content are used for disentangling fast electrons (with velocity $v \approx c > c/n$) from lower-velocity charge particles (e.g. pions with velocity $v < c/n$).

The Cherenkov detectors made of dense, optically transparent materials of large sizes can serve as an **Electromagnetic calorimeter** which measures the total energy of electrons and γ-quanta at high energies. This is achieved owing to the development of the electromagnetic cascading process in the calorimeter medium: a consecutive bremsstrahlung by high-energy electrons and conversion of γ-quanta into e^+e^- pairs. As a result, a definite fraction of the electron (or γ-quantum) energy is transformed to the Cherenkov radiation. The detection of the latter allows to measure the total energy of the incident electron (or γ-quantum).

A similar calorimetric principle is used in **Hadronic calorimeters**. They are made of a large-volume dense material (lead, tantalum, iron etc.) in which a number of scintillation or Cherenkov radiators are embedded. The dense material serves as a target, where the incoming high-energy hadron undergoes multiple inelastic interactions producing, in particular, a large number of π^0 mesons which decay into γ-quanta, $\pi^0 \to 2\gamma$. The latter convert into e^+e^- pairs which emit light in the radiator. The detection of this light allows measuring the total energy of the incident hadron.

Magnetic spectrometers are often used to measure the charged particle momentum, provided that its trajectory in the magnetic field is reconstructed with the help of detectors. The trajectory of a particle with momentum $\boldsymbol{p}$ and charge $Q = e \cdot q$ in a constant magnetic field $\boldsymbol{B}$ is a helix, with radius of curvature R. The latter is related to the momentum component $p_\perp$ perpendicular to $\boldsymbol{B}$ as

$$p_\perp = 0.3 \cdot q \cdot B \cdot R,$$

where the measurement units are GeV/c for $p_\perp$, Tesla for B and meter for R.

Chapter 9. *NA60 fixed target heavy ion experiment at CERN. Analysis of data on charged hadrons production in 158A GeV Indium-Indium central collisions.*

NA60, entitled "Study of Prompt Dimuon and Charm Production with Proton and Heavy Ion Beams at the CERN SPS", is one of the CERN heavy ion experiments at the SPS accelerator. The experimental programme of NA60 includes detection of μ^+- and μ^--leptons as well as charged hadrons: proton, antiproton, π^+-, π^--, K^+, K^-. Due to its Beam Tracker and Vertex Telescope subcomponents, NA60 allows a high-precision reconstruction of the primary interaction vertex, which in turn enables a high-resolution measurement of the momenta of the detected particles (see below). During the years 2002 - 2004 NA60 has collected data on the proton-ion and ion-ion collisions with various ions and at different beam energies. In this Chapter, we will describe the analysis of data on the charged hadrons production in the collisions of the Indium beam at energy of 158 GeV per nucleon with the fixed Indium target.

NA60 experimental setup

The NA60 experimental setup (Figure 9.1) is composed of four main detectors which are placed in the following order (along incident beam direction, i.e. along *z*-axis): silicon **Beam Tracker**, silicon **Vertex Telescope**, **Zero Degree Calorimeter** and **Muon Spectrometer** **.**

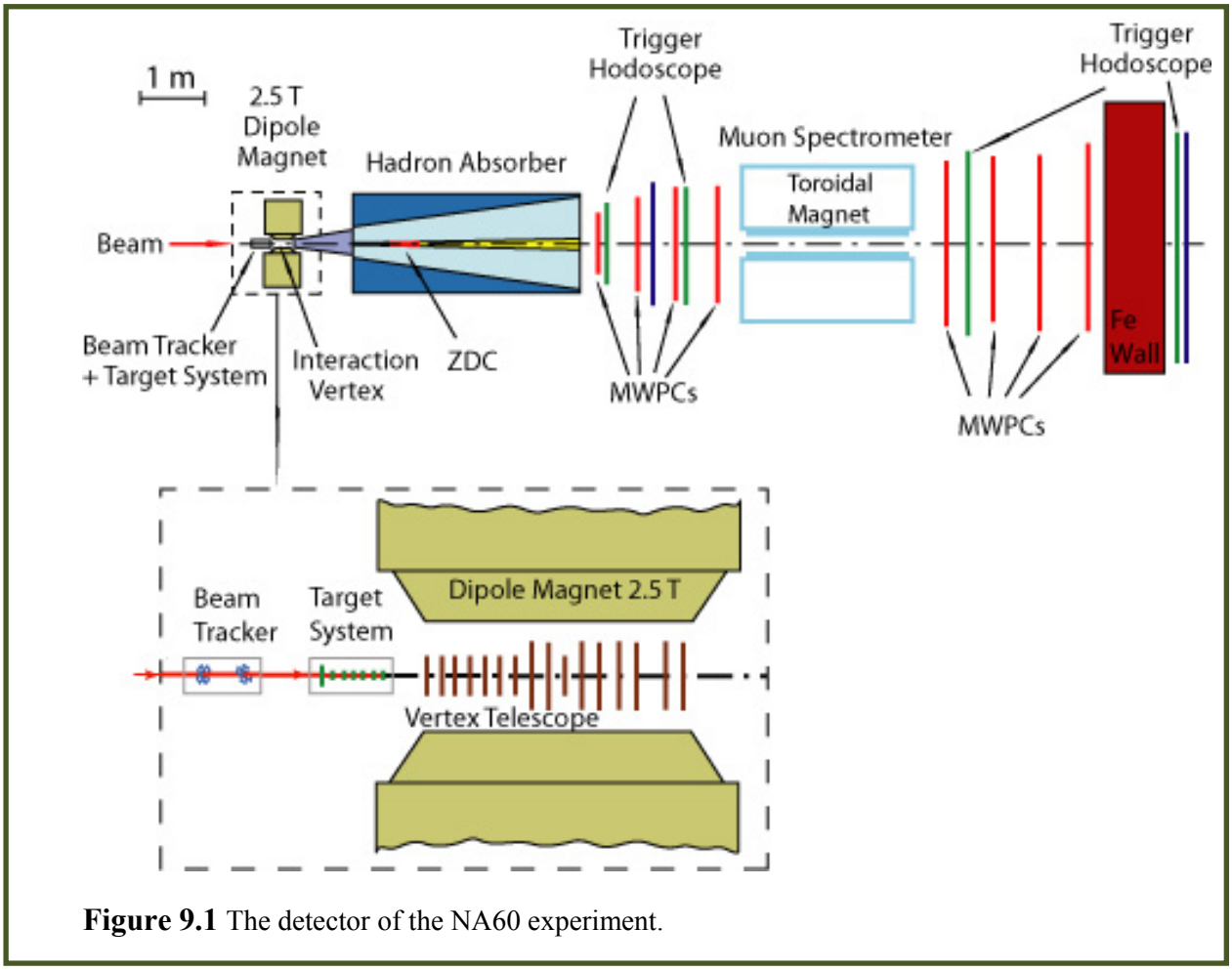

Figure 9.1 The detector of the NA60 experiment.

Beam Tracker (BT) consists of two planes of silicon strip detectors (placed perpendicularly to z–axis, being 20 cm apart along z–axis) both of which measure the transverse x– and y–coordinates of the beam particle with accuracy about 20 μm. This allows reconstruction of the beam particle trajectory. After passage through the BT, the beam particle can interact, with some probability, with the target system placed downstream of the BT.

Target System (TS) consists of 7 cylindrical subtargets (7.5 mm apart) with diameter 1 mm and thickness 1.5 mm, and made of indium (with the average atomic weight A=115). When a beam particle interacts in a subtarget, a number of secondary particles (mainly pions and kaons) are produced. For the case of the indium ion beam with energy E_0=158A GeV (i.e. E_0=158×115 GeV≈18 TeV), up to several hundreds particles can be produced.

Vertex Telescope (VT), located downstream of the Target System, provides the detection of a fraction of secondary charged particles produced in the polar angle interval $2^o \leq \vartheta \leq 5^o$ (ϑ is the angle between the particle momentum $\boldsymbol{p}$ and z–axis). The VT consists of 16 consecutive vertical planes composed of a large number of silicon pixel detectors, each of sizes 50 μm×425 μm, and allows reconstruction of the charged particle trajectories and coordinates of the primary interaction vertex, from where the particles originate. The VT is placed inside a 2.5 Tesla dipole magnet which bends the particle trajectory, hence allowing the measurement of its momentum, as well as the sign of its charge. A typical example of the registered and reconstructed event is demonstrated in Figure 9.2. Produced charged particles are registered in VT. The green lines, which converge to the interaction vertex, are the reconstructed tracks of these particles, while the yellow line follows the ion beam.

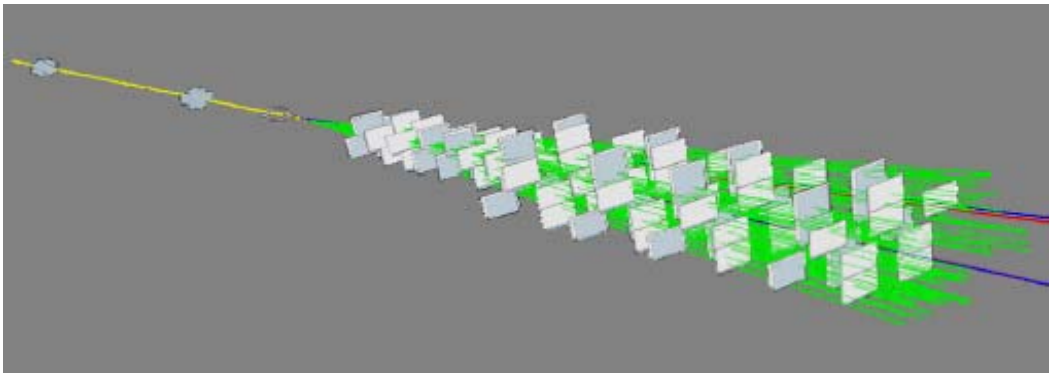

Figure 9.2 Display of a reconstructed event in the Beam Tracker and Pixel Telescope

Zero Degree Calorimeter (ZDC), located 1.5 m downstream of the VT, is dedicated to the measurement of the energy of non-interacting fragments of the incident nucleus. These fragments (light nuclei and nucleons) flow at almost zero angles relative to the beam direction. Hence the transverse size of the ZDC is chosen so that only the particles with very small angle ϑ ($\vartheta < 0.2^o$) can hit it. The ZDC is made of tantalum in which Cherenkov detectors (quartz fibers) are embedded. If the incident Indium nucleus does not interact in the Target system and hits the ZDC, the intensity of the collected Cherenkov light is maximal and corresponds to the kinetic energy of the incident nucleus, $E_{ZDC}^{\max} = T_0 \approx E_0 \approx 18$ TeV. Otherwise, the measured energy E_{ZDC} is proportional to the number of non-interacting (so called spectator) nucleons: $E_{ZDC} = N_{spect}$×158 GeV, while the number of interacted (participant) nucleons of the incident nucleus is equal to $N_{part} = \mathrm{A} - N_{spect}$. The extracted value of N_{part} serves as a measure of the collision centrality; the case of $N_{part} \approx \mathrm{A}$ (i.e. $N_{spect} << \mathrm{A}$ or $E_{ZDC} << E_0$) corresponds to very central collisions (when almost all nucleons participate in the interaction), while the case of $N_{part} << \mathrm{A}$ (i.e.

$N_{spect} \approx$ A or $E_{ZDC} \approx E_0$) corresponds to very peripheral interactions (when only a very small fraction of nucleons are participants).

Muon Spectrometer (MS) (placed downstream of the ZDC) is the largest detector of the NA60 setup. It detects muon pairs produced in In-In collisions. The MS consists of a toroidal magnet and several proportional chambers and scintillation detectors, which allow to identify muons, reconstruct their trajectories and measure their momenta. The MS is separated from the VT by a Hadron Absorber of 5 m length along z-axis. This absorber protects the MS from the flux of hadrons (mainly pions and kaons) produced in the interaction vertex, as well as reduces the flux of background muons from the decay of $\pi^{\pm}$ – and $K^{\pm}$ – mesons. The data from the MS are not used in the present work which is devoted to the study of the charged particle production, using the Vertex Telescope.

General selection criteria of NA60 In–In interaction events

The NA60 setup is irradiated by the beam of 158A GeV Indium ions with an intensity of $5 \cdot 10^7$ ions per 5 s. The time interval Δt between two neighbouring ions undergoes statistical fluctuations around its mean value Δt=5 s /$5 \cdot 10^7$=100 ns. On the other hand, the time interval τ_{vt} necessary to read information from the Vertex Telescope is 238 ns. During this time, more than one ion can interact in the Target System leading to an overlapping of the interaction patterns reconstructed by the VT. These, so called "pile–up" events should be rejected.

Another source of deterioration of the interaction characteristics arises when, after an interaction of an ion in a subtarget, its spectator fragments interact in one or more downstream subtargets and loss a fraction of their energy before being detected in the ZDC. This makes impossible to estimate correctly the number N_{part} of nucleons participated in the initial In–In collision. These, so called "secondary interaction" events also should be excluded.

By these and some other reasons the following general criteria of event selection are applied:

1. The summary energy E_{ZDC} of non–interacting nucleons of the projectile is smaller than $E_{ZDC} < E_0 = 158 \times 115$ GeV=18 TeV. Note, that for central In–In collisions (considered below) a more strict cut is applied, E_{ZDC}<7 TeV, corresponding to N_{part}>70.

2. Not more than one ion is detected in BT within the ZDC gate time (10 ns).

3. Not more than one ion is detected by the BT during the time interval τ_{VT}=238 ns necessary to read information from VT.

4. Only one interaction vertex is reconstructed (with the help of charged particle tracks detected in VT) in one subtarget (out of 7 subtargets). The transverse coordinates of that vertex are compatible with those extracted by extrapolation of the ion trajectory (reconstructed by the BT) up to the subtarget where the interaction had taken place.

NA60 event sample used for the study of the particle multiplicity fluctuations

As it was already mentioned in Section 7, one of the signatures of the QGP formation is the enhanced (non-statistical) fluctuations in the multiplicity of particles produced in central nucleus-nucleus collisions, where the most part of nucleus nucleons participate the interaction and a large number of hadrons (mostly pions and kaons) are produced. In NA60 experiment, about third of charged particles, produced in the 158A GeV In–In collisions, are detected by the VT having a full angular acceptance $2^o < \vartheta < 5^o$.

The further step is the choice of the range of the azimuthal angle φ, defined as $\varphi = arctg(p_y / p_x)$, where p_x and p_y are the particle momentum components in the transverse plane. In general, the distribution on φ in the full range of $-\pi < \varphi < \pi$ is expected to be uniform, when it is averaged over a sufficiently large number of events.

However, in practice the apparatus effects can deteriorate this uniformity. In particular, the VT detector of the NA60 setup covers the domains $-\frac{11}{12}\pi<\varphi<-\frac{1}{12}\pi$ and $\frac{1}{12}\pi<\varphi<\frac{11}{12}\pi$. Besides, in these domens the geometrical efficiency ε of the particle detection somewhat depends on φ.

Due to these apparatus effects, the distribution on φ deviates from a flat one, as it can be seen from Figure 9.3, where the φ-distribution in the range $\frac{1}{12}\pi<\varphi<\frac{11}{12}\pi$ is plotted. As it is seen, the maximal efficiency ε_{max} of the particle detection is reached at $\frac{5}{12}\pi<\varphi<\frac{6}{12}\pi$ (the 5th bin of the histogram), for which we put $\varepsilon(\varphi)=\varepsilon_{max}=1$, while the minimal ε is reached at $\frac{10}{12}\pi<\varphi<\frac{11}{12}\pi$ (the 10th bin of the histogram) for which $\varepsilon(\varphi)=0.64$. Similarly, the values of $\varepsilon(\varphi)$ for other bins can be determined. The values of $\varepsilon(\varphi_i)$ (i=1, 2,...10), extracted from Figure 9.3, will be used in further analysis to take into account the apparatus effects (see below).

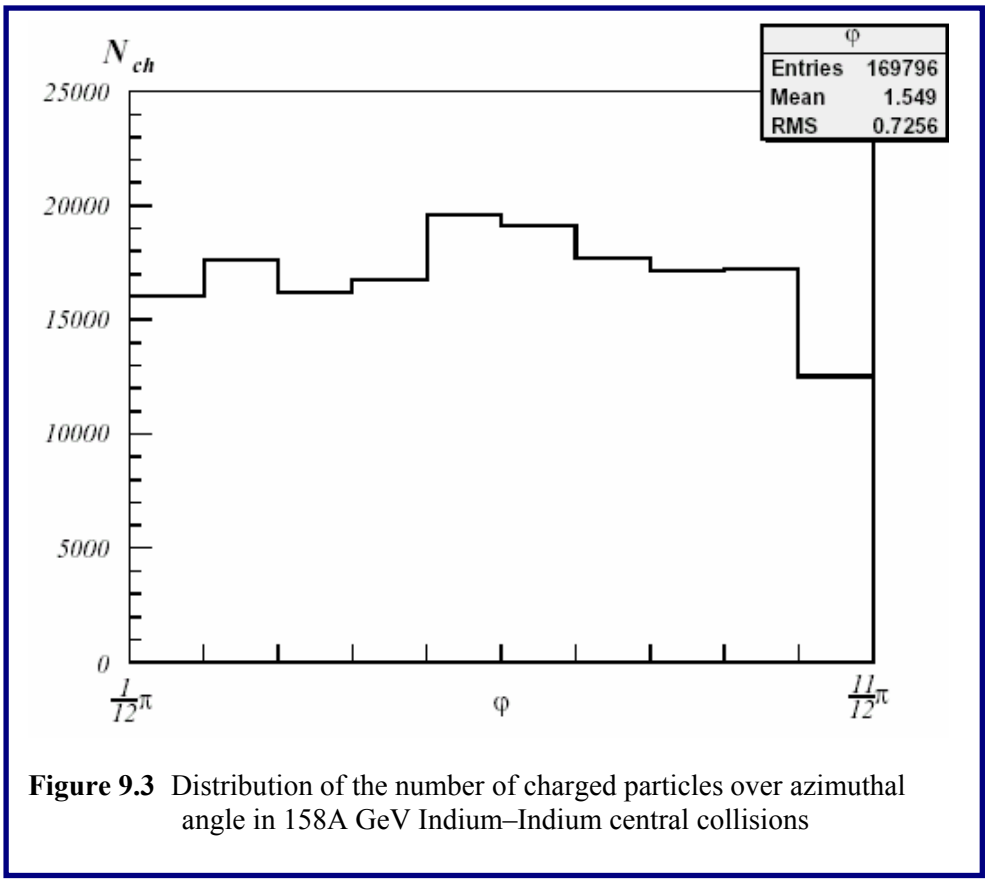

Figure 9.3 Distribution of the number of charged particles over azimuthal angle in 158A GeV Indium–Indium central collisions

The final step of the event selection is the choice of central collisions for which $E_{ZDC} < 7\,\text{TeV}$, corresponding to $N_{part} = 70$ participant nucleus (out of A=115) of the incident In nucleus and the mean impact parameter $\bar{b}$ of the collision $\bar{b}$=3fm (the impact parameter is the distance between centers of colliding nuclei in the plane perpendicular to the beam direction).

Besides, we require that the number of produced charged particles is sufficiently large (in order to get a statistically provided φ-distribution for each event), namely, $n \geq 25$ in the chosen domain of the polar angle.

The total number of events of the central In–In collision satisfying the event selection criteria is equal to $N_{tot} = 3284$.

Search for the multiplicity fluctuations over azimuthal angle in NA60 data on 158A GeV Indium–Indium central collisions

The aim of this work is an event-by-event analysis of the multiplicity distribution over the azimuthal angle in central In–In collisions. The analysis is done using the NA60 data at the energy of 158A GeV. Enhanced dynamical (non-statistical) multiplicity fluctuations are expected in case of the QGP formation and they have to be disentangled from the statistical ones, which are inherent to any stochastic process.

Let the considered φ-domain is divided into M equal bins. The probability to find a produced particle in the i-th bin (i = 1,...,M) is equal to $q_i=\varepsilon_i f$, with ε_i being the particle detection efficiency for the i-th bin and f=1/M.

Let us assume now that the particles are produced independently in the considered φ-domain and their total number equals N_0. Then, in the absence of dynamical fluctuations, the probability $P(n_i)$ that the i-th bin is occupied by n_i particles (out of N_0) obeys the binomial law:

$$P(n_i) = C_{N_0}^{n_i} q_i^{n_i} (1-q_i)^{N_0-n_i} \tag{9.1}$$

where $C_{N_0}^{n_i}$ is the number of combinations of n_i elements out of N_0. It is easy to check that the probabilities $P(n_i)$ satisfy the normalization condition

$$\sum_{n_i=0}^{N_0} P(n_i) = 1 \tag{9.2}$$

The mean value of n_i is equal to

$$\overline{n}_i = \sum_{n_i=0}^{N_0} n_i P(n_i) = N_0 q_i \tag{9.3}$$

while its mean square deviation (dispersion) from the mean $\overline{n}_i$ (characterizing the spread of the distribution) is

$$\sigma_i^2 = \sum_{n_i=0}^{N_0} (n_i - \overline{n}_i)^2 P(n_i) = N_0 q_i (1-q_i) \tag{9.4}$$

Let now an event is registered with N_{ev} particles detected in the considered φ-domain and distributed over M bins as $n_1, n_2, ..., n_M$ ($N_{ev} = \sum_{i=1}^{M} n_i$). Due to a limited detection efficiency ($\varepsilon < 1$), N_{ev} is smaller than the number N_0 of produced particles. The most probable value of N_0 can be determined assuming that the originally produced N_0 particles are randomly distributed over M bins with the corresponding known probabilities q_i. The value of N_0 should satisfy the requirement that the observed values of n_i deviate minimally from the expected mean values, $\overline{n}_i$. In the mathematical statistics, the deviation is characterized by the sum

$$U = \sum_{i=1}^{M} \frac{(n_i - \overline{n}_i)^2}{\sigma_i^2} = \sum_{i=1}^{M} \frac{(n_i - N_0 q_i)^2}{N_0 q_i (1-q_i)} \tag{9.5}$$

with the values of $\overline{n}_i$ and σ_i^2 taken from Eqs. (9.3) and (9.4) and with $q_i = \varepsilon_i f$. It can be shown that the minimal value of U is reached at

$$N_0^2 = \sum_{i=1}^{M} \frac{n_i^2}{\varepsilon_i(1-f\varepsilon_i)} \Big/ \sum_{i=1}^{M} \frac{f^2\varepsilon_i}{1-f\varepsilon_i} \qquad (9.6)$$

which is expressed through the experimentally observed numbers n_i and known quantities of f and ε_i (i=1,...,M).

Inserting the value of N_0 from (9.6) into (9.5), one obtains the minimal value, $U_{\min}$, of U. It is more convenient to deal with the value of $U_{\min}$ per bin, i.e. with the normalized quantity $U_{norm} = U_{\min}/M$ (note, that in our analysis the number of bins is set to M=10).

In the absence of dynamical fluctuations, it is expected that the U_{norm} – distribution has mean value $\overline{U}_{norm}$ slightly smaller than 1, with a shape rapidly falling in the region of U_{norm}>1 (see below).

As compared to the statistical fluctuations, the dynamical ones can cause larger values of U_{norm} for the following reason. In case of large fluctuations, the occupancy n_i for some bins is noticeably larger, while for the other bins it is noticeable smaller, than the mean value $\overline{n}_i = N_0 q_i$ (Eq. (9.5)). Large deviations of n_i from $\overline{n}_i$ result in higher probabilities for large values of U_{norm}, e.g. at $U_{norm} > 2$ (i.e. in the "tail" region of the distribution). As a result, the mean value and the dispersion of U_{norm} have to exceed the values expected for the case of purely statistical fluctuations.

In order to make clear whether the experimental U_{norm}–distribution contains other than statistical fluctuations, we should compare it with a so-called U_{stat}–distribution. The latter is obtained with artificial (simulated) events for which the azimuthal angles are randomly, independently and uniformly distributed over M bins, taking into account the φ–dependence of the detection efficiency $\varepsilon(\varphi)$. Each simulated event has its own corresponding event (with the same number N_0 of produced particles) in the real event sample. The values of U_{stat} for simulated events are calculated in the same way as for U_{stat} for real events. Finally, the obtained U_{stat}-distribution for simulated event sample is compared with the experimental U_{norm}–distribution. Any statistically provided difference between these two distributions, at large values of U (e.g. $U > 2$), can serve as an evidence for dynamical fluctuations which can be caused, according to theoretical predictions, by the QGP formation.

The distributions of U_{norm} for the central In–In collisions and those of U_{stat} for the simulated events are plotted in Figure 9.4. In the experimental distribution, no enhancement is observed in the "tail" region as compared to the U_{stat}-distribution.

It should be noted that in distribution over the azimuthal angle we do not observe dynamical fluctuations when φ-domain is divided into M = 15 bins or when we require that the number of produced charged particles is more large ($n \geq 50$ instead of $n \geq 25$)

The main conclusion of this work is that one did not observe significant dynamical fluctuations in central In–In collisions. As the probability of the QGP formation is predicted to increase with the growth of the number N_{part} of participant nucleons (i.e. with the decrease of $\overline{b}$), it is not excluded that the dynamical fluctuations can appear at very central collisions, i.e. for the sample of events with a more severe restriction on E_{ZDC}. Such a kind of analysis requires, however, a larger statistics of events than it is available at present.

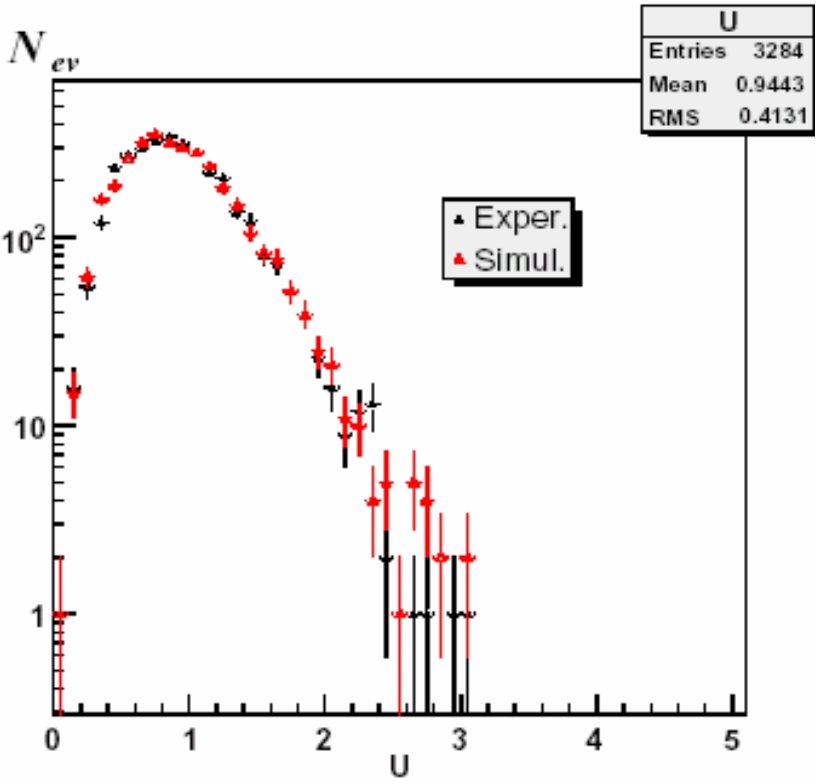

Figure 9.4 *U*–distribution for real and simulated events

Acknowledgements

We are deeply grateful to:

- Professor Ara Grigoryan, President of the Armenian e-Science Foundation and leader of the ALICE group of YerPhI, Drs Hrant Gulkanyan, leading scientific researcher and chief of laboratory #143 of YerPhI, Ruben Shahoyan, member of NA60 Collaboration, CERN, Martin Poghosyan, member of the ALICE/YerPhI group, as well as Artem Harutyunyan and Arsen Hayrapetyan, members of the Armenian e-Science Foundation and ALICE/YerPhI group, for continuous help and encouragement in the course of preparation of this textbook;

- Personnel of the laboratory #143 and ALICE/YerPhI and NA60/YerphI groups, for thoughtful attitude;

- Swiss Fonds Kidagan and Calouste Gulbenkian Foundation from Lisbon, for the financial support of our work and studies

Literature

1. ***Particle Data Group*** "Review of Particle Physics" Physics Letters B592 (2004) pp 1-1109

2. ***Введение в Физику Высоких Энергий,*** Перкинс Дональд (Москва Энергоатомиздат 1991)

3. ***A Brief History of Time***, Stephen W. Hawking (Bantam Press, 1988).

4. ***From Quarks to the Cosmos: Tools of Discovery***, Leon M. Lederman and David N. Schramm (Scientific American Library, 1989).

5. ***The Particle Odyssey: A Journey to the Heart of Matter,*** Frank Close, Michael Marten, Christine Sutton (Oxford University Press, 2002)

6. ***Introduction To Elementary Particles***, David Griffiths (John & Sons, New York 1987)

7. ***The First Three Minutes,*** Steven Weinberg (Basic Books, Inc., Publishers, New York 1988)

8. ***Слабое Взаимодействие Элементарных Частиц,*** Лев Б. Окунь (Москва Физматгиз 1963)

The following web sites were very helpful

http://hepweb.rl.ac.uk/ppUKpics/pr_powarch.html

http://www.lbl.gov/abc/

http://www.cpepweb.org/

http://particleadventure.org/particleadventure/

http://na60.cern.ch/

http://aliceinfo.cern.ch

http://www.wikipedia.org

http://physics.nist.gov/cuu/index.html